International Journal of Powertrains

ISSN online: 1742-4275 - ISSN print: 1742-4267
https://www.inderscience.com/ijpt

Evaluation of electrified airpath configurations for an opposed piston two stroke compression ignition architecture

Erik Vorwerk, Patrick O'Donnell, Dennis Robertson, Robert Prucka, Benjamin Lawler, Fabien Redon, Ming Huo, Ashwin Salvi

DOI: 10.1504/IJPT.2024.10059544

Article History:

Received:	11 September 2022
Last revised:	16 February 2023
Accepted:	17 August 2023
Published online:	16 April 2024

Evaluation of electrified airpath configurations for an opposed piston two stroke compression ignition architecture

Erik Vorwerk*, Patrick O'Donnell, Dennis Robertson, Robert Prucka and Benjamin Lawler

Department of Automotive Engineering,
Clemson University,
4 Research Drive, Greenville, SC 29607, USA
Email: evorwer@clemson.edu
Email: odonne9@clemson.edu
Email: dennis.m.robertson@gmail.com
Email: rprucka@clemson.edu
Email: bjlawle@clemson.edu
*Corresponding author

Fabien Redon, Ming Huo and Ashwin Salvi

Achates Power Inc.,
4060 Sorrento Valley Blvd.,
San Diego, CA 92121, USA
Email: redon@achatespower.com
Email: huo@achatespower.com
Email: salvi@achatespower.com

Abstract: Opposed piston two-stroke (OP2S) diesel engines have shown promise in reducing emissions and increasing efficiency compared to conventional four-stroke diesel engines. Airpath design on this architecture is critical to realising these benefits, as OP2S scavenging and internal composition are primarily controlled by intake and exhaust pressure differentials, and most pumping work is incurred external to the engine cylinder. Using 1-D simulation and an experimentally validated baseline model, this research evaluates the influence of airpath design on steady-state performance metrics of a two-cylinder OP2S engine. First, conventional, electrified, and novel compression and expansion devices are considered, as well as a range of scavenging control devices, to develop four viable airpath architectures. These architectures are then compared across their operating ranges, and a sensitivity analysis is performed on various airpath component efficiencies. Overall, it is found that the best layout investigated consists of an electrically assisted turbocharger with a variable geometry turbine.

Keywords: opposed piston two stroke; two-stroke; OP2S; electrified airpath; sensitivity analysis; electrified turbocharger; compression ignition; diesel engine; pumping work; scavenging control.

Reference to this paper should be made as follows: Vorwerk, E., O'Donnell, P., Robertson, D., Prucka, R., Lawler, B., Redon, F., Huo, M. and Salvi, A. (2024) 'Evaluation of electrified airpath configurations for an opposed piston two stroke compression ignition architecture', *Int. J. Powertrains*, Vol. 13, No. 1, pp.19–53.

Biographical notes: Erik Vorwerk is a PhD candidate in Automotive Engineering at Clemson University where he also earned his MS in Automotive Engineering in 2022. His research revolves around novel and conventional diesel engines in both hybrid and conventional powertrains, with a focus on airpath design and transient engine control.

Patrick O'Donnell is a Post-Doctoral appointee with the Multi-Physics Computation group at Argonne National Laboratory. He received his PhD in Automotive Engineering from Clemson University in 2023. His current research focuses on alternative fuels for large-bore rail applications.

Dennis Robertson is a Principal Research Scientist at LinQuest where he focuses on data analysis and machine learning. He received his PhD in Automotive Engineering from Clemson University where his doctoral work included developing control-oriented combustion models for spark assisted compression ignition. Prior to this, his work was primarily experimental combustion research for advanced spark-ignited engines.

Robert Prucka is the Alan Kulwicki Professor of Motorsports Engineering within the Department of Automotive Engineering, the Director of the Deep Orange vehicle prototyping program, and the Deputy Director of the Virtual Prototyping of Autonomy-Enabled Ground Systems Centre (VIPR-GS) at Clemson University. His teaching and research interests include the design, control, calibration, performance, and emissions of advanced powertrain systems. He is currently researching the use of artificial intelligence and/or optimal control strategies for the design and operation of electrified powertrains used in autonomous off-road vehicles. He earned his PhD in Mechanical Engineering from the University of Michigan in 2008.

Benjamin Lawler is an Associate Professor in the School of Mechanical and Automotive Engineering at Clemson University. His research is related to renewable fuels for internal combustion engines, advanced combustion strategies to minimise pollutant emissions and maximise efficiency, alternative engine architectures or technologies to minimise heat transfer losses, and hybrid vehicle strategies that work collaboratively with his other research interests to provide sustainable transportation and power generation solutions for human civilisation. His graduate degrees were from the University of Michigan.

Fabien Redon is currently CTO and EVP Product Development at Westport Fuel Systems, responsible for Engineering, Product Development and Program Management. For the duration of the work covered in this article he was EVP and CTO at Achates Power where he led opposed piston engine development. Prior to his time with Achates Power, he was responsible for the production development of light duty diesel engine powertrains for General Motors. Before that for Detroit Diesel he was the technical interface between Daimler headquarters in Germany and Freightliner for the development of medium duty trucks for the US after spending time developing new diesel engines for the light duty vehicles. He holds a BS in Mechanical Engineering from Florida Institute of Technology, a MS in Automotive Engineering from the University of Michigan, and an MBA from the University of California San Diego.

Ming Huo assumes the role of Chief Engineer and Program Manager at Achates Power, which specialises in opposed piston engine development for a range of applications with the goal of reducing emissions and providing robust compliance in a cost-effective manner. He has been responsible for the combustion system development for a few key programs in the company, including the hydrogen opposed piston engine program. He graduated from Zhejiang University before receiving his MS and PhD at the University of Illinois at Urbana Champaign.

Ashwin Salvi completed his PhD in Mechanical Engineering at the University of Michigan, studying the thermo-physical properties of nano-carbonaceous layers in heat exchangers, evaluating optimal control strategies for hybrid vehicles, and diving into research based in thermodynamics and heat transfer. He joined ARPA-E at the US Department of Energy as a Fellow in 2013, where he worked on high-risk, high-reward energy concepts. He then joined Achates Power, where he led customer engagements, won more than $40 M in competitive federal contracts, and commercialised novel high-efficiency power generation technology.

1 Introduction

Recently, opposed piston two stroke (OP2S) diesel engines have seen significant research to investigate their potential advantages over comparable two-stroke and four-stroke diesel engines (Abani et al., 2017). Both two-stroke and OP2S engines can achieve a greater power density than a four-stroke engine due to their increased power stroke frequency, reducing the required displacement for a given application (Heywood and Sher, 1999). OP2S engines also use piston-operated ports, negating the need for a valvetrain, and simplifying the engine (Kalke et al., 2014). Both of these benefits help offset the packaging and complexity downsides of requiring a second crankshaft and geartrain on an OP2S engine, leading to an engine with comparable packaging and favourable complexity compared to a conventional four-stroke engine (Sokolsky and Major, 2019). Having two opposing pistons per cylinder also allows for the intake and exhaust ports to be located at opposite ends of the cylinder. This allows for more favourable uniflow scavenging without the need for poppet valves, potentially allowing for improved efficiency over a conventional two-stroke engine (Mattarelli et al., 2018). The OP2S architecture also has potential paths for reducing in cylinder heat transfer, which can lead to additional efficiency benefits. This is achieved in two primary ways: firstly, each pair of pistons face each other and share a common cylinder, negating the need for a cylinder head. This can lead to a lower heat transfer area and lower coolant heat rejection (Herold et al., 2011). Secondly, since each pair of pistons in an OP2S share a cylinder, the effective mean piston speed for a given total effective stroke length is halved. This allows for larger stroke-to-bore ratios and a reduced heat transfer area during combustion without exceeding mean piston speed limits (Kalke et al., 2014). A final potential benefit of the OP2S architecture is the ability to widely control internal residual ratios through airpath actuators (Patil et al., 2018). This allows for strategies such as increasing internal residual and decreasing external EGR to increase exhaust temperatures during cold start and low-load operation to improve catalyst light-off times

and increase catalyst conversion efficiencies, reducing tailpipe emissions (Redon et al., 2015).

These potential advantages may allow OP2S engines to increase diesel fuel efficiency and power density while also reducing tailpipe emissions compared to conventional four-stroke diesels. However, further research is necessary to address the challenges OP2S engines must overcome to see widespread commercial adoption. These challenges primarily centre around durability, mainly due to lubrication and thermal management (Pirault and Flint, 2010), and emissions control, mainly due to gas exchange complexity, oil consumption, and fuel injection challenges (Regner et al., 2011). Of these challenges, this work focuses on addressing the complexity of controlling the gas exchange process through the evaluation and investigation of different airpath configurations and devices.

Historically, OP2S engine airpaths have primarily focused on efficiently meeting intake pressure and airflow requirements, using various methods, including piston operated pumps (Witzky et al., 1965), conventional superchargers (Pirault and Flint, 2010), electrified turbochargers (Young et al., 2021), turbines mechanically coupled to the engine (Indig and Haman, 1985), and dual-stage turbocharger-supercharger combinations (Timoney, 1969; Mazuro and Kozak, 2022). While this has resulted in some relatively efficient OP2S designs, there has generally been little focus until recently on developing airpaths that allow for the complicated gas exchange process of an OP2S engine to be accurately controlled (Salvi et al., 2022; Gainey et al., 2022). This work focuses on not only how to select components for an efficient OP2S airpath but also on what considerations need to be made to design an airpath that allows for broad and efficient control of the gas exchange process.

This paper first provides an overview of the OP2S gas exchange and scavenging process. Airpath requirements for OP2S engines are then discussed, as well as what devices on the market can meet these requirements. These discussions drive the selection of four airpath layouts and the creation of a 1D model to investigate their performance. These layouts utilise different combinations of compression and expansion devices, some of which are mechanically or electrically driven, to achieve sufficient control over the gas exchange process and to meet airflow requirements. These layouts are compared across the engine's operating range on a pumping work, torque output, and control authority basis before the two most promising layouts are selected for further analysis. A sensitivity study is then performed on these layouts to determine the sensitivity of brake thermal efficiency (BTE) to various airpath component efficiencies.

1.1 OP2S scavenging process

Before selecting airpath components to investigate, it is important to understand how scavenging occurs in an OP2S and why controlling the scavenging process is a significant challenge of OP2S engines. Since two-stroke engines lack dedicated exhaust and intake strokes, the scavenging process must occur in roughly one-third of the time of a four-stroke engine. To allow sufficient time for scavenging to occur, the intake and exhaust valves or ports of a two-stroke engine have substantial opening overlap by design. Figure 1 compares flow area and cylinder volume for the breathing events of a conventional four-stroke engine with poppet valves and an OP2S engine with piston-operated ports starting at top dead centre firing (TDCf).

The blowdown process starts at a similar crank angle for both architectures. However, the OP2S gas exchange process fully completes before the intake valves on the four-

stroke begin to open. This short gas exchange window leads to the significant overlap in a two-stroke architecture and the gas exchange process occurring during relatively little piston motion. This means that a two-stroke engine lacks the positive displacement exhaust process of a four-stroke. The lack of a positive displacement process to push out exhaust gas and pull in fresh charge means that the pressure difference between the intake and exhaust manifolds is the primary factor driving the scavenging process.

Figure 1 Comparison of the effective flow area and cylinder volume of an OP2S and conventional four-stroke diesel of similar per-cylinder displacement (see online version for colours)

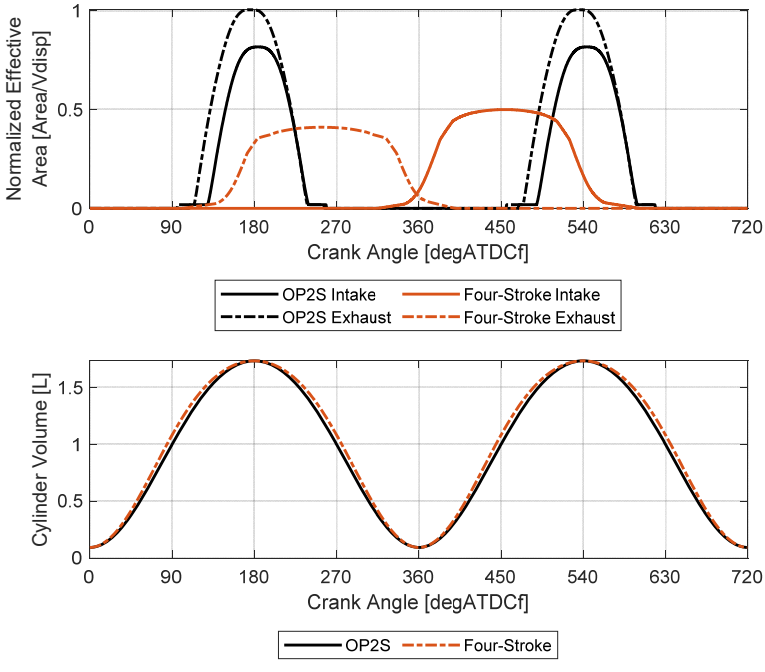

Notes: Two engine cycles are shown for the OP2S, and one engine cycle is shown for the four-stroke architecture. the OP2S has a significantly shorter time for the gas exchange process and, therefore, has a much larger valve overlap.

Since the scavenging process of an OP2S is driven by pressure differentials, OP2S engines are significantly more sensitive to intake and exhaust pressures than their four-stroke counterparts (Gainey et al., 2022; Liu et al., 2017). Changes in these pressures lead to significant changes in internal composition, which can greatly impact efficiency and emissions. For example, in some operating conditions of the OP2S used for this study, a 10 mbar reduction in delta pressure (dP) across the engine leads to a 20 K increase in peak cylinder temperature, a 2bar increase in peak cylinder pressure (PCP), and a 10 K increase in exhaust gas temperature. This concept is also represented in Figure 2, where a four-stroke engine and an OP2S of identical per-cylinder displacements were run at the same speed, fuelling, and EGR fraction at a range of intake pressures and dPs. In the context of this paper, dP is described as the difference between the intake manifold or chest pressure and the exhaust manifold or chest pressure averaged across one engine cycle. Due to fundamental geometric differences between the OP2S and four-stroke, the

changes in dP have a much greater influence on flow through the engine and internal composition. The OP2S also has a narrower range of dPs at which it can run since this architecture requires a higher intake pressure than exhaust to drive flow.

While dP ultimately controls the scavenging process in an OP2S engine, this term doesn't describe how an OP2S is scavenging. To represent the scavenging performance of an OP2S, multiple parameters can be used as outlined in Appendix A, with the most relevant terms for this work being

1 scavenging efficiency (SE)
2 scavenging ratio (SR) (Blair, 1996).

Figure 2 Comparison of normalised intake mass flow rate (MFR) vs. dP for an OP2S and a conventional four-stroke diesel engine with similar per-cylinder displacement (see online version for colours)

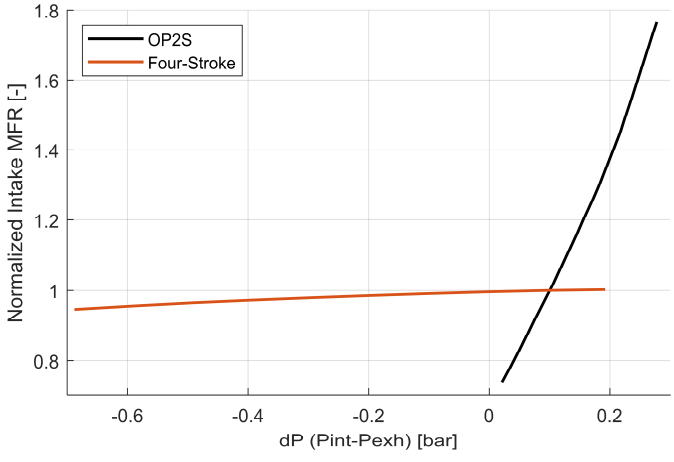

Notes: the OP2S architecture shows a higher sensitivity to dP and a narrower range of viable dPs, pointing to the need for accurate airpath control

$$\text{SE} = \frac{\text{Mass of delivered mixture retained}}{\text{Mass of trapped cylinder charge}} \leq 1 \tag{1}$$

$$\text{SR} = \frac{\text{Mass of delivered mixture}}{\text{Mass of trapped cylinder charge}} \geq \text{SE} \tag{2}$$

In these equations, 'delivered mixture' refers to the mixture of air and external EGR entering the cylinder through the intake, and 'trapped cylinder charge' refers to the mixture trapped in the cylinder at port/valve closure consisting of all burnt and unburnt species, including internal residual, external residual, and air.

SE is a metric of how well the delivered mixture displaces the burnt charge from the previous engine cycle. A higher SE will lead to less internal residual, while a lower SE will lead to more internal residual. The SR describes how the mass of the delivered mixture relates to the total trapped mass at port/valve closure. When the SR > 1, the engine ingests more mixture than can be trapped in its cylinder, and some flow escapes into the exhaust. Ideally, an engine's SR will equal its SE. This implies that the delivered mixture perfectly displaces the burnt charge from the previous cycle, and none of the delivered mixture escapes into the exhaust (Blair, 1996). This leads to reduced pumping

work and is one of the reasons the uniflow scavenging allowed by the port design of an OP2S is beneficial (Gainey et al., 2022; O'Donnell et al., 2022). Controlling the SR and SE through dP also allows for the internal residual of an OP2S to be widely controlled, allowing for some of the benefits described in the introduction to be realised. This, along with the other side effects of an OP2S engine's high sensitivity to intake and exhaust system pressures, points to the need for a well-optimised airpath with independent intake and exhaust pressure control to realise the potential benefits of the OP2S architecture fully.

2 Airpath component selection and evaluation

The airpath of a modern OP2S has three primary goals. The airpath must be able to meet intake pressure and airflow requirements efficiently, it must be able to meet EGR targets efficiently, and it must be able to control engine dP to meet engine scavenging targets efficiently. The following sections detail the process followed to meet the above goals and select the four final airpaths investigated in this study.

2.1 Selection of compression and expansion devices

While intake pressure and airflow targets could be met without recovering energy from the exhaust, this would lead to a significant efficiency penalty. Therefore, this goal is broken down into three subtasks:

1 Recover as much energy as possible from the exhaust gas while retaining sufficient control over backpressure

2 Efficiently use this recovered energy to compress the intake charge

3 Efficiently add/subtract additional energy to achieve intake pressure and airflow targets.

Two main classes of expansion devices are considered to fulfill subtask one: centrifugal expanders and positive displacement expanders. Thermo-electric generators (Lion et al., 2017; Orr et al., 2016), organic Rankine cycle waste heat recovery systems (Alshammari et al., 2018), and other systems are not considered for this study.

Centrifugal expanders are commonly used as the expansion devices on conventional turbochargers. However, they can also power an electric generator (Lee et al., 2017; Ricardo et al., 2011) or be mechanically coupled to the engine (Indig and Haman, 1985; Amann, 1987). The primary advantages of this class of expanders are their compact size, high efficiency, and broad operating range. The main disadvantages are their high operating speeds, making engine or electric machine coupling more complex, their poor energy recovery and transient response at low engine speeds and loads, and their potential for surge and over-speeding at high engine speeds and loads. Due to their commercial availability and benefits, centrifugal expanders are investigated further in the final airpaths.

Positive displacement expanders fall into two main categories: piston expanders (Andruskiewicz et al., 2021a, 2021c) and rotary expanders (Amann, 1987). Piston expanders generally utilise a piston coupled to the main crankshaft of the engine to expand out the exhaust gasses from the fired cylinders. This method benefits from fast

transient response and efficient work transfer to the crankshaft. However, this expander requires a complete engine redesign and has poor low-load performance, primarily due to friction. Additionally, it is unclear from literature whether the fundamental gas exchange differences of a two-stroke engine are compatible with this type of expander. Due to these complications, this type of expander was not chosen for this study. Rotary positive displacement expanders generally use a screw, vane, or scroll architecture to expand the working fluid. They are commonly used in organic Rankine cycle waste heat recovery applications (Alshammari et al., 2018). However, they have historically been considered for direct recovery of engine exhaust energy as well (Sekar and Kamo, 1983). This class of expanders can allow for reasonable control over system backpressure, operate at lower shaft speeds, are less prone to over-speeding, and are generally more efficient during low-load operation than centrifugal expanders (Amann, 1987; Sekar et al., 1984). While previous literature has shown promise for positive displacement expanders, these studies were primarily simulation-based, and this class of expanders has yet to see commercial adoption for direct recovery of exhaust energy. Therefore, it was omitted from further analysis in this work.

The process of compressing the intake charge to fulfill part of subtask 2 can generally be done in either one or two stages. A significant advantage of two-stage compression when using turbochargers is that it allows for greater transient response than a larger single-stage turbocharger while still maintaining intake pressure requirements (Serrano et al., 2008). Two-stage compression setups can also allow for greater flexibility when sizing boost devices, allowing for one device to be optimised for lower MFR requirements and the second device to be optimised for higher MFRs (Bassett et al., 2016). These benefits of two-stage boosting can be partially negated through the use of an electrically assisted turbocharger (EAT). The EAT motor can supply extra power to the compression device on demand, significantly improving transient and low-speed response (Lee et al., 2017). Two-stage boosting also has the advantage of allowing for higher boost pressures to be more efficiently achieved (Galindo et al., 2010; Zhang et al., 2013). For the OP2S used in this study, the engine was operated at an average boost pressure of 2.25 barabs, so this benefit is likely less impactful than it would be for architectures with higher boost levels. Ultimately, both single and two-stage boosting layouts were considered in the final airpaths to investigate how the potential benefits of two-stage boosting compare with advanced electrified single-stage boosting designs.

Fulfilling subtask 2 also requires transferring the energy recovered by the expansion device(s) to power the compression device(s). This transfer can be done either electrically or mechanically, with each strategy having its benefits and drawbacks (Lee et al., 2017). Having the devices mechanically coupled allows for reduced losses compared to an electric coupling, but this generally comes at the expense of independent control over the compressor and expander speeds. Having these devices electrically coupled allows for independent control of compression and expansion device speeds, which in turn allows for reasonable control over system pressures, but this comes at the expense of greater conversion losses. An electrical coupling can also allow for easier recovery and storage of excess expansion energy when the expansion power is higher than the compression power.

For the final architectures, a mechanical coupling between primary expansion/compression devices was used for two primary reasons: Firstly, a scavenging control actuator, such as a variable geometry turbine (VGT), can be used to control system pressures with mechanically coupled devices. Secondly, for the tested

architecture, the required compression power is always higher than the potential expansion power. This means that there is never a situation where there is excess expansion energy that could be recovered in a battery or other storage system. For these reasons, an electrical coupling would likely be less efficient than a mechanical coupling, and the test engine would only be able to utilise the potential benefits of an electrical coupling partially.

Both positive displacement and centrifugal compressors were considered in determining the type of compression device(s) for the single and two-stage boosting systems. Centrifugal compressors are most commonly used for conventional turbochargers, but they have also seen increased use in electrically driven superchargers (Lee et al., 2017; Bassett et al., 2016). Centrifugal compressors generally have better high speed/high load performance than positive displacement rotary compressors, at the expense of slower transient performance depending on the drive mechanism. Since they are not positive displacement, they also have a non-linear response to rpm which can increase control complexity. Due to their commercial availability and benefits, centrifugal compressors are investigated further in the final airpaths.

Positive displacement compressors are generally either piston based (Pirault and Flint, 2010; Witzky et al., 1965; Andruskiewicz et al., 2021b) or rotary (Lee et al., 2017). Piston compressors have a separate piston connected to the engine's crankshaft operating at the same speed as the main power pistons of the engine. One compression piston generally feeds two power cylinders for four-stroke engine designs, where each revolution of the compression piston provides compressed charge to one power cylinder. While this design shows promise for mid and high-load operation, it is generally inefficient at low loads, and its fixed speed relative to the crankshaft presents control limitations. Additionally, as is the case with piston expanders, it requires a complete redesign of the engine to integrate. For these reasons, this architecture was omitted from further analysis. Rotary positive displacement compressors generally utilise either a roots or twin-screw architecture. The primary benefit of these types of compressors is their low-speed efficiency and fast transient response. However, this comes at the expense of relatively low peak efficiency and the need for decoupling the compression device speed from engine speed to prevent over-boosting at high speeds. Due to their low-speed benefits and transient response, rotary positive displacement compressors were investigated further in the final airpaths that utilise two-stage compression.

Electrical and mechanical drives were considered to provide the additional power to a compression device required to meet subtask three. Mechanical drives allow for fewer parasitic losses. However, they generally require adding a second compression device and generally couple engine speed to compression device speed. Recent developments, such as mechanical super turbo chargers, are an exception to these generalities, allowing for variable-speed mechanical coupling with a single boost device at the expense of greater conversion losses (Ricardo et al., 2011). Electrical drives generally have greater speed flexibility and can be implemented on the primary boost device or a secondary device. However, their conversion losses are generally greater than their mechanical counterparts. (Lee et al., 2017). Since both types of power delivery methods show promise for the airpath investigations, both mechanical and electric drives were implemented in the tested layouts to explore which set of trade-offs was more beneficial.

2.2 Selection of EGR devices and layout

All layouts in the final investigation share a similar EGR system. This was done to reduce the number of variables between airpath layouts and because the EGR path has a relatively small influence on pumping work compared to the primary boost devices. However, since the influence on pumping work is not negligible, a study is presented to determine what type of EGR system and loop is more efficient for the test engine.

There are two primary classifications of EGR loops: high-pressure and low-pressure. In a high-pressure EGR loop, exhaust gas is circulated from upstream of the expansion device(s) in the exhaust to downstream of the compression device(s) in the intake. On average, this method leads to a shorter EGR path length and generally leads to better transient response than a low-pressure loop (Zheng et al., 2004). However, since the OP2S architecture requires a higher intake than exhaust pressure, an EGR pump is necessary to implement this pathway. In a low-pressure EGR loop, exhaust gas is circulated from downstream of the expansion device(s) to upstream of the compression device(s). This layout generally has a worse transient response than a high-pressure loop, but it can negate the need for an EGR pump and allows for exhaust gas to be re-circulated from downstream of the after treatment system, reducing intake fouling (Zheng et al., 2004). The two EGR layouts also have different implications for airpath efficiency. These implications were investigated in 1D simulation software. The architecture for this investigation is similar to layout A, described in a following section. The two tested configurations are as follows:

1 Low-pressure loop from downstream of the turbine to upstream of the compressor. This loop utilises a valve for control and has an EGR cooler to reduce intake charge heating

2 High-pressure loop from upstream of the turbine to downstream of the compressor. This loop utilises an electric EGR pump for control and an EGR cooler upstream of the pump to increase pump efficiency. An electric EGR pump was chosen for its ease of control, although there may be negligible efficiency differences compared to a mechanically driven pump.

For the test engine, the high-pressure EGR loop is more efficient than the low-pressure loop, even though it requires an electric EGR pump. This difference is caused by how the EGR flow affects the primary boost devices. Utilising a low-pressure EGR loop increases the MFR through the turbine and compressor by up to 40%, depending on the operating condition. This excess exhaust flow is expanded by the turbine generating work to compress it with the compressor. However, this is an inefficient process for two reasons. Firstly, because the EGR must travel through multiple expansion/compression devices, the efficiency of each process combines to yield a low overall compression efficiency compared to a dedicated EGR pump. Secondly, the EGR heats the intake charge, making the compressor operate less efficiently. The combination of these efficiency penalties exceeds that of using an electric EGR pump. Therefore, a high-pressure loop with an electric EGR pump is utilised in the final layouts.

2.3 Selection of dP and scavenging control devices

To efficiently control engine dP, and therefore scavenging, a scavenging control actuator is needed. The scavenging control actuators in this work have a specific SR target to meet for a given operating condition and utilise a similar basic mechanism to achieve this target: To reduce the SR of the engine, it is necessary to reduce the amount of air + EGR entering the cylinder. To do this while maintaining the same internal composition requires increasing the internal residual so that less external residual/EGR is necessary. This can be achieved by lowering the dP across the cylinder, i.e., controlling the intake and exhaust pressures to be closer so that less burnt charge is pushed out, in conjunction with raising the intake pressure so that the same mass of air (not including EGR) can enter the cylinder. To increase the SR, the opposite is true; the engine must be operated at a higher dP to push out more internal residual so that the MFR of air + EGR into the cylinder increases. However, changing the dP to match the scavenging target can incur an efficiency penalty, as flow must be restricted, increased, and/or rerouted.

Figure 3 Comparison of the relative brake efficiency of different scavenging ratio control strategies across their feasible control ranges (see online version for colours)

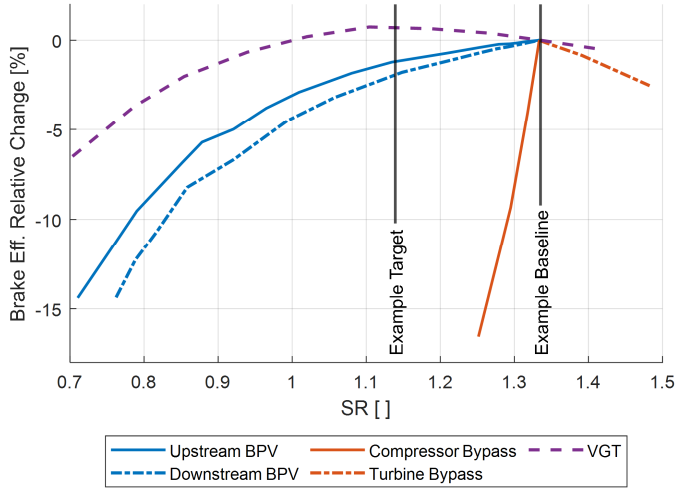

Notes: Most devices have a significant efficiency penalty when controlling the scavenging ratio below/above the baseline value.

In evaluating a scavenging control device, the trade-off between this efficiency penalty and the scavenging control range of the actuator must be considered. To fairly compare this trade-off, the test engine is set up as follows for all five tested actuators: Engine speed, injected fuel mass, trapped air, and trapped mass quantities are kept consistent across the sweeps. This allows for the indicated thermal efficiency (ITE) at a given SR to be held constant between control strategies. This method is chosen as it allows for the differences in BTE between control devices to be compared. The control devices share a common engine architecture and airpath layout based on layout 'A,' discussed in Figure 4. For the example operating point shown in Figure 3, the test engine has a baseline SR of approximately 1.32 with no control device and a target SR of approximately 1.14. The target SR is derived from previous projects, and its determination is outside this work's

scope. These baseline and target SR values will also differ at different operating conditions, but the general trends described for each device will still hold true.

An exhaust backpressure valve (BPV) can be located either upstream or downstream of the turbine. A variable restriction can be placed on the exhaust by varying the valve angle, changing the dP and allowing the SR to be lowered below the baseline value, as shown in 3. The primary benefit of a BPV is its large pressure control window. However, this control range comes at a significant efficiency penalty. Additionally, a BPV can not be used to increase the SR of an engine beyond its fully opened setting.

It is also shown that an upstream BPV performs better than a downstream BPV. The reason for this is twofold. First, the turbine is more efficient when operated at a higher pressure ratio. In the case of the upstream BPV, the pressure downstream of the turbine is approximately ambient (1 bar), so the pressure ratio is equal to whatever the pressure is upstream of the turbine. However, in the downstream BPV case, because the BPV is downstream of the turbine, the pressure downstream of the turbine is greater than ambient. This means that even when operated at the same absolute pressure drop across the turbine, the upstream BPV turbine will be more efficient because it operates at a higher pressure ratio. The second main reason for the greater efficiency with an upstream BPV is that turbine efficiency tends to increase as the reduced MFR increases. Reduced MFR has units of (mass flow rate*temperature0.5)/turbine inlet pressure; thus, a lower absolute pressure entering the turbine will trend towards higher efficiency. Since the upstream BPV causes a pressure drop upstream of the turbine, the absolute pressure entering the turbine is lower than in the downstream BPV case, leading to higher efficiency.

Although a BPV is not the most efficient scavenging control device, its relative simplicity and control range make it a promising scavenging control actuator. An upstream BPV was therefore investigated further in one of the tested airpath layouts (Figure 4).

A compressor bypass is a valve that allows compressed charge leaving the turbocharger compressor to be bypassed back upstream of the compressor. Bypassing air around the compressor to lower the SR leads the EAT to operate at a higher speed to meet the constraints described earlier. Since the compressor and turbine are coupled in this architecture, this leads to the turbine speed increasing as the SR decreases. This also leads to a lower MFR in the exhaust, as the internal residual is higher, and short-circuiting decreases at a lower SR. The combination of these effects causes the turbine's operating point to shift towards a higher pressure ratio. This higher pressure ratio means that the turbine is placing more of a restriction on the exhaust, lowering the SR.

While this device does allow for some scavenging control (Figure 3), it was not used as a scavenging device on the evaluated airpaths for two primary reasons. Firstly, it has the worst trade-off between a change in SR to a change in BTE at the tested conditions. Secondly, it has the narrowest control range out of the investigated devices, limiting the potential benefits of having control over engine scavenging.

A turbine bypass, also known as a wastegate, allows exhaust gases to be redirected around the turbine. This has the effect of lowering the restriction placed on the exhaust by the turbine, increasing the dP, and leading to a higher SR (Figure 3). This device shows promise for scavenging control when the engine is under scavenged. However, it has a relatively poor trade-off between a change in SR to a change in BTE, and increasing the SR is not desirable since the test engine is over scavenged during most operating

conditions. The combination of these two drawbacks means that a turbine bypass is not a viable solution for scavenging control on this architecture by itself. Therefore, other more promising solutions were pursued for the evaluated airpaths.

A VGT uses a similar principle to the BPV to influence scavenging. By varying the vane angles, the effective restriction caused by the turbine changes, changing the engine's dP and the SR. Since the full pressure drop in the exhaust is still occurring across the turbine, the turbine can recover this energy, leading to the lowest observed efficiency penalty (Figure 3). Since this device has the greatest scavenging control range and lowest efficiency penalty, it was further investigated in some of the tested airpath layouts.

3 Investigated airpaths

Using these insights on airpath components and coupling methods as guidance, four airpath layouts were developed to fulfill the three primary goals of an OP2S airpath (Figure 4).

Figure 4 Airpath layouts investigated. components within the dotted boxes are changed between layouts (see online version for colours)

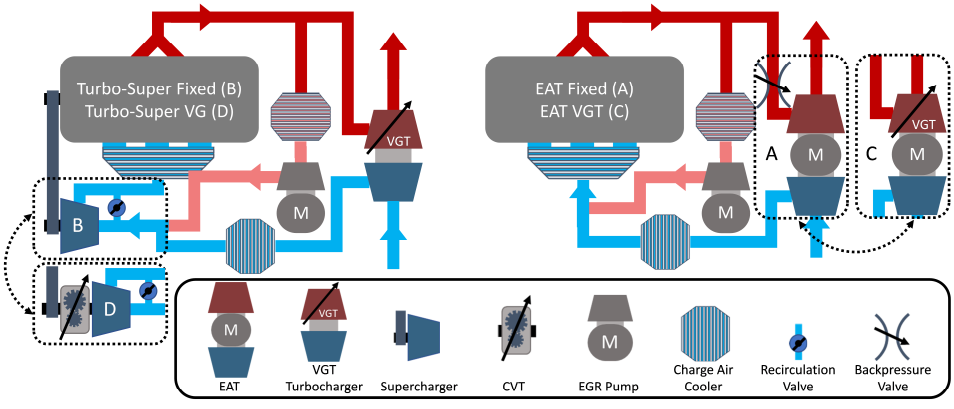

Notes: all layouts share a common engine architecture and a common EGR layout to provide a more direct comparison between airpath layouts.

3.1 Layout A (EAT fixed)

This layout consisted of a single-stage boost device with a high-pressure EGR loop and a back pressure valve (BPV) upstream of the turbine on the exhaust side. The boost device for this layout was a mechanically coupled EAT with fixed turbine and compressor geometry. This EAT was sized and developed specifically for this architecture and featured a 15 kW peak electrical assist. Using an EAT allowed for the boosting requirements of the engine to be met with a single device, negating the need for a secondary compression device. The high-pressure EGR loop used an electrically driven positive displacement pump to overcome the pressure differential between the intake and exhaust, while the upstream BPV provided the necessary control over engine dP to meet scavenging targets.

3.2 Layout B (turbo-super fixed)

This layout consisted of a two-stage boosting system with a high-pressure EGR loop identical to layout A. The first stage of the boosting system was a conventional turbocharger with a VGT, allowing for control over engine scavenging. The second stage was a positive displacement supercharger mechanically driven by the engine through a single-speed gearbox. An external bypass valve was used to allow for excess flow from the supercharger to be recirculated upstream of the supercharger, preventing over-boosting at high engine speeds. The turbocharger and supercharger for this model were developed on a different OP2S project (Redon et al., 2015) and resized appropriately for this application.

3.3 Layout C (EAT-VGT)

This layout was similar to layout A with a couple of key differences. The BPV was removed, and the EAT turbine was replaced by the VGT from Layout B. In this layout, the scavenging control was therefore accomplished using a VGT. This layout was designed to investigate if using a VGT instead of a BPV is feasible for scavenging control on an EAT and if a VGT can mitigate the efficiency penalties associated with a BPV.

3.4 Layout D (turbo-super CVT)

This layout was similar to layout B with one key difference. The single-speed gearbox driving the supercharger was replaced with a CVT with an assumed efficiency of 88%. Literature has shown that a CVT's efficiency depends on multiple factors, including speed and torque (Verbelen et al., 2017). However, an average efficiency of 88–90% was shown to reasonably account for losses under most operating conditions, although this efficiency may be as high as 93% under certain situations (Boretti, 2019). A later section discusses the influence of this assumed efficiency value on the brake efficiency of the test engine. The goal of this layout was to investigate if the additional control and reduced reliance on a supercharger recirculation valve afforded by the CVT outweighed the increased mechanical losses of this system.

4 1D modelling approach

To evaluate the airpaths shown in Figure 4 and to provide the previously discussed insight in the 'airpath component selection and evaluation' section, a 1D simulation model was created using GT-POWER. The model used in this study was adapted from a three-cylinder OP2S 1D model that was experimentally validated to the test engine described in Naik et al. (2015). This model was validated across its operating range to predict steady state intake manifold pressure, exhaust manifold pressure, and air MFR within $\pm 1.5\%_{rel}$ on average, crank angle resolved cylinder pressure within $\pm 2.5\%_{rel}$ on average, and BTE within $\pm 2.5\%_{rel}$ on average. For this study, the three-cylinder model was converted into a two-cylinder architecture while retaining the same piston, cylinder, and port design as the three-cylinder model. A general overview of the specifications of this engine is shown in Table 1.

Table 1 General specifications of the OP2S engine investigated in this study

Cylinders	2
Pistons	4
Nominal displacement	3.3 L
Bore and combined stroke	98.5 mm × 215 mm
Swept compression ratio	18.7:1

As of the time of writing, the 1D simulation software used for this study does not natively support engines utilising multiple pistons or crankshafts per cylinder. Each pair of pistons sharing a common cylinder was instead modelled as a single piston with an imposed position profile. This profile is generated offline and is equal to the absolute distance between each pair of opposing pistons as a function of crank angle. This method allowed phenomena such as crank lead to be modelled and produced a volume trace equivalent to the physical engine.

Cylinder heat transfer was modelled using Woschni (1967). Due to the required method for modelling the cylinders and pistons, the mean piston speed predictions (MPS) were doubled, necessitating a reduction in the overall convection multiplier of this heat transfer model. The magnitude of this reduction was calibrated with experimental data, and the result was found to be sufficiently accurate for this study.

To account for the different frictional characteristics of an OP2S compared to a conventional four-stroke engine, a friction model of the following form was developed (3).

$$FMEP = A + B \cdot P_{max} + C \cdot mps + D \cdot P_{PC} + Q \cdot mps^2 + R \cdot P_{pC}^2 \quad (3)$$

where

P_{max} is peak cylinder pressure

mps stands for mean piston speed

P_{PC} is port closing pressure

A, B, C, D, Q, R are fit coefficients.

One of the key differences in this friction model as opposed to a model such as Chen-Flynn (1965), was the inclusion of the port closing pressure term, which was found to be a significant influencer of engine friction during the experimental development and calibration of this model.

The OP2S engine model utilised a large number circumferentially located piston operated ports as detailed in O'Donnell et al. (2022). Due to the shape of these ports, each port was modelled with an imposed area profile, allowing for the small flow area present when the rings have cleared the ports, but the top land was still restricting the flow area to be represented. This was an important area of the gas exchange process to model on an OP2S as it is when a significant portion of the backflow into the intake can occur.

The combustion process was modelled using a predictive direct-injection diesel multi-pulse model that was adapted from the validated three-cylinder 1D model described previously. This model was coupled with a combination of measured and interpolated injector rate maps to approximate injector performance.

4.1 Modelling the scavenging process in 1D simulation

A challenging aspect of modelling an OP2S in 1D simulation is accurately representing mixing during the gas exchange process. Since there is a significant period where both intake and exhaust ports are open, a large portion of the fresh charge entering the cylinder can directly escape through the exhaust ports. This means that it is necessary to model what portion of the mixture leaving through the exhaust is burnt gas, and what is fresh charge, to accurately predict internal composition. The default option to model this in the 1D simulation software used is to impose an exhaust residual ratio (ERR) vs. cylinder residual ratio curve on the engine, where ERR is the fraction of mass leaving the cylinder into the exhaust that is burned. Previous work has found a reasonable agreement using this method for OP2S engines (Mattarelli et al., 2017). However, the following method using a SE-SR correlation provided a better agreement with experimental data for the tested architectures.

As a surrogate for 3D CFD modelling, a simplified correlation relating to SE and SR was used to approximate the experimental engine's scavenging performance across its normal operating range. Using a SE-SR correlation to represent engine scavenging has three main benefits (Heywood and Sher, 1999; Liu et al., 2017):

1 For an engine with fixed geometry, a single SE-SR correlation will be valid for that engine independent of engine speed and load

2 A SE-SR correlation allows for the complex flow fields in two-stroke scavenging to be captured in a temporally and spatially averaged manner

3 A SE-SR correlation is continuous and can be created by fitting data to relatively simple equations.

These benefits mean that a small subset of data from experimental work, or 3D CFD simulations, can be used to generate a SE-SR correlation that allows for a 1D model to predict scavenging performance across an engine's operating range accurately. A detailed description of SE-SR correlations and their validity is available in Appendix B. SE-SR correlations were used in this work to model engine scavenging in the following way:

Like the default method described previously, the scavenging methodology used for this work determines what the correct ERR of the cylinder should be at a given operating condition. However, instead of determining ERR based on the cylinder residual ratio, ERR was instead based on the error in the SE of the model. On a per-cycle basis, the SE and SR were calculated within the 1D simulation. The calculated SR was then input into the SE-SR correlation of the engine to predict what the actual SE of the engine should be. Depending on the error between the calculated and predicted scavenging efficiencies, a controller then either increased or decreased the ERR for the next cycle. This process continued until the measured and calculated scavenging efficiencies converged to within 2% of each other.

Using the above method allowed for the benefits of 1D and 3D simulation to be leveraged. The higher fidelity 3D CFD was used to characterise the highly spatially/temporally varying scavenging process of an OP2S and generate data to fit the SE-SR correlation. At the same time, the faster runtime and lower modelling complexity of 1D simulation allowed for complete systems to be simulated and modified relatively quickly.

5 Targets and actuators for the simulations

To determine which airpath is more efficient, it is important to quantify the various airpath-related losses. To provide a representative comparison of the engine architectures and losses, it was desired to hold trapped mass, trapped air, and injection parameters constant. This allowed for ITE to be held approximately constant across layouts, allowing for the pumping losses to be more easily compared. Since trapped air and trapped mass were difficult to control directly, the following parameters were targeted instead using the actuators in Table 2. Targeting trapped AFR allowed for the trapped air in the cylinder to be held constant for a given fuelling. When combined with a trapped burned fraction target, this also allowed for the total trapped mass to be held constant. Finally, targeting a SR allowed for the MFR through the engine to be kept consistent.

Table 2 Simulation targets and actuators. ( ) indicate layouts using a given actuator

Target	*EAT actuator (A, C)*	*Turbo-super actuator (B,D)*
Load	Total injected mass	
Fuelling	Pilot and main masses	
	Pilot and main SOIs	
	Fuel rail pressure	
Trapped burned fraction	EGR pump speed	
Trapped AFR	EAT speed	SC bypass valve position (B) or CVT ratio (D)
Scavenging ratio	BPV position (A) or VGT rack (C)	VGT rack and BPV position

The load was controlled by changing the total injected mass (mg/cyl/cyc) of the engine. The total injected mass was broken into pilot and main injections based on the engine speed and total desired fuelling. The fuel rail pressure was also changed depending on the engine speed and total fuelling, influencing the injector rate shape.

Trapped burned fraction is the fraction of burned inert gas at intake port closing, not including residual burnt air from lean combustion. It is controlled by varying the EGR pump speed to increase or decrease the external EGR rate until the trapped burned fraction is within 1% of the target.

Trapped AFR is the air-fuel ratio calculated using the total trapped air, including residual air, and the total injected mass, as shown in (4)

$$\text{Trapped AFR} = \frac{\text{Total trapped mass} * \left(1 - \text{trapped burned fraction}\right)}{\text{Injected fuel mass}} \tag{4}$$

The trapped AFR target was achieved by varying the air MFR into the cylinder. Air MFR could be modulated by one of three means depending on the layout: EAT speed (layouts A and C), supercharger bypass valve position (layout B), or supercharger speed via the CVT's gear ratio (layout D). These methods controlled the trapped AFR to within 0.2 points of the target.

The SR was calculated using (2). Using the BPV position (layout A) or VGT rack position (layouts B-D), the exhaust backpressure was modulated to hold the SR to within 1% of the target value.

The specific targets for this simulation were generated using an experimental OP2S engine and an experimentally validated 1D model of the same engine. From these sources, target maps were created based on total injected mass and engine speed for the parameters described above. This methodology was followed to develop targets that were experimentally shown to have acceptable engine out emissions, as emissions are not predicted in 1D simulation.

6 Results

The results presented in the following sections were generated by simulating the layouts across their operating ranges from 700–2,500 rpm and 15–155 mg/cyl/cyc fuelling in a 323-point grid. Points that fulfilled the convergence criteria described in the previous section and did not violate any mechanical constraints were then extracted for further analysis. In the resulting valid data points, the ITE was within 0.3%rel on average between layouts at a given speed/fuelling. This error was likely due to variations in controller convergence and was relatively insignificant compared to the differences in pumping losses between layouts.

Figure 5 Parasitic losses relative to available fuel energy for the tested layouts (lower = better) averaged across their common operating ranges (see online version for colours)

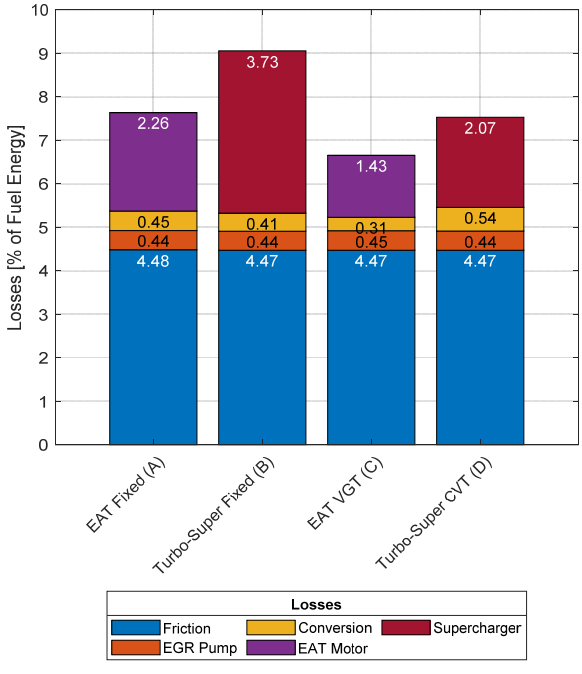

Notes: The control strategies used allow for frictional and EGR pump losses to remain approximately constant. This allows for the boosting and conversion losses to be directly compared.

Since the ITE of the layouts was approximately equivalent, any BTE changes will result from either pumping work or frictional losses. Since the OP2S lacks a pumping loop, the

pumping losses are equivalent to the work required to operate the EGR pump and any boost devices on the engine. Figure 5 breaks down the average pumping and frictional losses across the operating ranges for the investigated layouts.

An important note from Figure 5 is that while the frictional and EGR pump losses across the various layouts had some slight differences due to controller convergence variation, these differences were insignificant relative to the magnitude of other losses. This means that any changes in BTE or BSFC observed will be primarily a result of the boosting devices and SR control strategies. Because of this, the losses of the boost devices and their associated conversion losses can be analysed separately, as shown in Figure 6.

Figure 6 Comparison of the boosting devices and conversion losses from Figure 5 (lower = better) (see online version for colours)

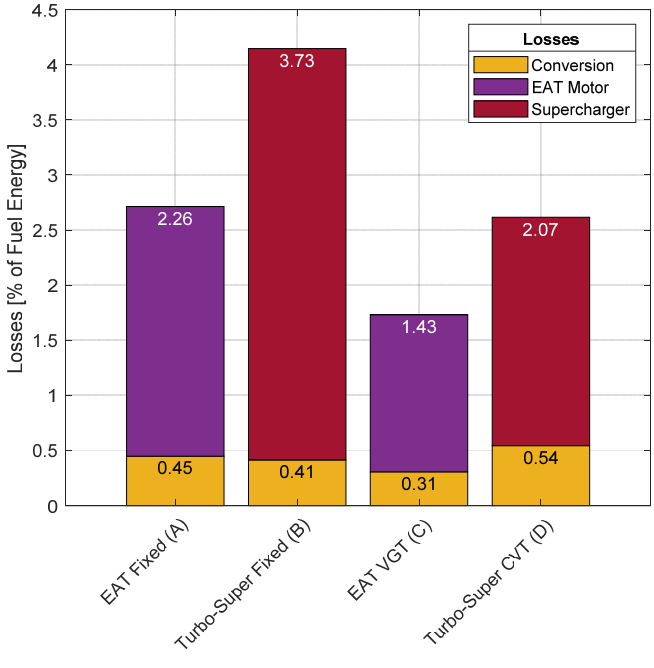

Notes: The conversion losses include all losses incurred from transferring power at the crankshaft to power at the boost device. The boost device losses are measured at the boosting devices themselves.

Overall, layout B had the highest airpath losses. This was primarily due to the control strategies necessary to operate a supercharger with a fixed gear ratio on the test engine. Since the supercharger speed in this layout was coupled with engine speed, the supercharger must be sized and use a gear ratio that meets a worst-case boost requirement, generally high-load low-speed, and then use a recirculation valve to modulate boost pressure for airflow control elsewhere in the operating range. This valve recirculates any excess air from the high-pressure to the low-pressure side of the supercharger, maintaining the target boost pressure. Since up to two-thirds of the flow through the supercharger must be re-circulated at low load, additional pumping losses

were incurred compared to the other layouts. This is shown in the total supercharger losses in Figure 6 and in the higher mechanical power of the supercharger itself compared to layout D, as shown in Figure 7.

These losses could be reduced by lowering the gear ratio of the supercharger, but this also would reduce the maximum airflow through the supercharger, limiting peak torque. These limitations with a fixed gear supercharger follow conclusions in literature and are one of the driving factors in developing variable speed superchargers such as is utilised by layout D (McBroom et al., 2012; Turner et al., 2015). The fixed gear ratio of the supercharger also made it more sensitive to supercharger sizing. Previous iterations of layouts B and D utilised larger superchargers. Moving to the supercharger size used for this study reduced the average boosting device losses of layout B by ~50%, while the same change yielded a negligible effect on layout D. While the variable drive ratio in layout D made it less sensitive to supercharge sizing, it did have one major limitation: its conversion losses. The turbo-super CVT had the highest conversion losses relative to its required boost device power of any layout (Table 3), limiting the potential efficiency benefits of this airpath.

Figure 7 Average mechanical power of the expansion and compression devices of the tested layouts (see online version for colours)

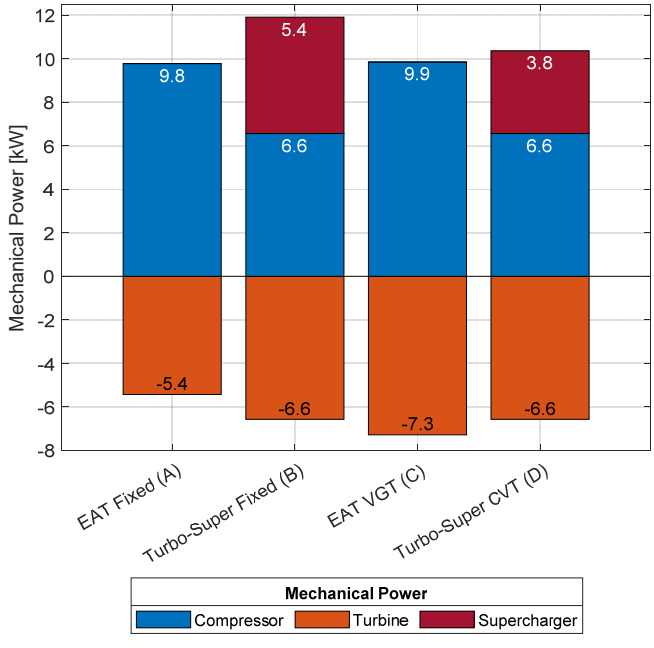

Notes: While layouts a and c have similar compression requirements, the backpressure valve of layout a reduces the energy recovered by the turbine.

Of the two EAT layouts (A and C), the EAT VGT architecture had 37%$_{rel}$ lower and 32%$_{rel}$ lower boost device and conversion losses respectively on average. Since these layouts both had single-stage boost devices, the difference in losses must manifest within either the compressor or turbine of their respective EATs.

Table 3 Average percentage of energy lost to conversion losses relative to total boosting device energy

Layout	*Relative conversion losses [%]*
EAT fixed (A)	16.6
Turbo-super fixed (B)	10.0
EAT VGT (C)	17.7
Turbo-super CVT (D)	20.8

As discussed previously, these layouts shared the same compressor, and their air delivery requirements are the same due to the previously discussed targets. Therefore, the power required to drive the compressor should remain constant between the layouts at a given speed and fuelling. On average, the compressor power requirements were within $1\%_{rel}$ between these layouts, as shown in Figure 7. This means that the differences in pumping losses must manifest in another area of the system.

On average, the VGT of layout C was 10%rel more efficient and recovered 34%rel more energy from the exhaust compared to the conventional turbine of layout A (Figure 7). These differences were the primary causes of the observed difference in boost device losses between layouts since this additional energy recovery means less electrical energy needed to be supplied by the EAT motor. The improved performance of the turbine on layout C was primarily due to the BPV on layout A. As was discussed previously, the BPV leads to a lower turbine efficiency by reducing the turbine pressure ratio and changing the reduced MFR through the turbine. An additional side effect of the BPV not discussed previously was that it reduces the amount of exhaust energy available for the turbine to recover since it imposes a pressure drop in the exhaust. This energy reduction was estimated using (5). On average 8% of the available exhaust energy leaving the cylinders was lost to the BPV, mainly at high load and low speed.

$$Q = mC_v\left(T_2 - T_1\right) + \frac{P_2V_2 - P_1V_1}{1-\gamma} \tag{5}$$

The difference in conversion losses shown in Figure 6 was due to the additional EAT motor power required to compensate for the loss in recovered turbine energy in layout A. The fraction of energy lost to energy conversions was comparable between layouts A and C (Table 3); thus, a higher EAT motor power leads to higher absolute conversion losses. The slightly higher relative conversion losses of layout C were due to the EAT motor being less efficient at the lower power levels of layout C, but this difference was relatively insignificant compared to the absolute difference in required power. Overall, these results follow the conclusions of the scavenging control device study (Figure 3), where a VGT was more efficient than a BPV for scavenging control.

7 Full map results

Up to this point, results have been discussed in the context of average pumping losses and airpath device work. Airpath selection also greatly influences an engine's overall performance and operating window. These influences can be helpful in deciding which of the investigated airpaths is most promising for a given application. The brake specific

fuel consumption (BSFC) for each of the four layouts as a function of brake torque and speed is shown in Figure 8 and Figure 9. The maximum torque for each of these airpaths was limited by three main factors: PCP, boost device power, and boost device speed. All else equal, it is generally desirable for an engine's output to be limited by its PCP, as this means that the airpath can supply sufficient air to meet the mechanical limits of the engine. When an engine is boost device power limited, the components supplying power to the compressor and/or supercharger cannot supply sufficient power to maintain trapped AFR targets. This can be due to gearing limitations or electric motor limitations. When an engine is boost device speed limited, sufficient power is available to drive the compressor, but the boost device is overspeeding and cannot match trapped AFR targets. The limiting factor in peak torque for each airpath is also plotted in Figure 8 and Figure 9.

For a large portion of the operating range, the fixed and VGT EAT layouts had a similar BSFC. The EAT VGT layout was significantly more efficient as the load increases or the speed decreases. This trend is related to the BPV. At low engine speeds there was more time for fresh charge to flow into the cylinder, promoting over-scavenging. At high engine loads the engine was operating at a higher boost pressure, which promoted more flow into the cylinder and potentially more over-scavenging. During these conditions the scavenging control device was used more heavily to reduce engine scavenging to the target values, leading to a large efficiency penalty in the case of the BPV. This trend is shown in Figure 10. Areas where high BPV losses were encountered correspond to the areas in Figure 8 where the EAT fixed architecture was less efficient.

Figure 8 BSFC comparison of layouts a (left plot) and c (right plot) (see online version for colours)

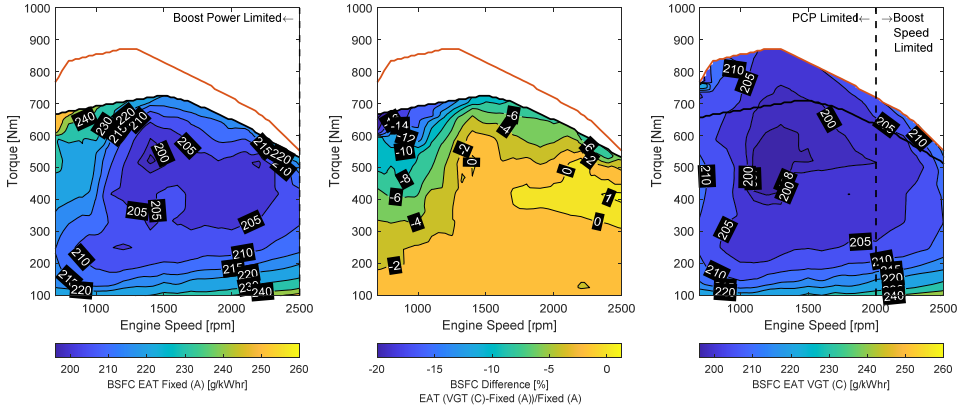

Notes: The middle plot shows the relative percent difference between the layouts, with a negative value corresponding to layout c being more efficient. Due to the BPV, layout a is significantly less efficient than layout c at high loads and low speeds

This large amount of energy lost to the BPV valve was also why the peak torque of the EAT fixed layout was significantly lower than that of the EAT VGT layout. At high loads, the EAT motor in layout A could not supply sufficient power to the compressor since less energy is being recovered by the turbine, preventing the trapped AFR target from being met and leading to the boost power limited torque curve in Figure 8. These

downsides associated with using a BPV could be lessened with geometric changes to the engine to make the engine over-scavenge less; however, as seen in Figure 3, a BPV will always have a worse efficiency trade-off than a VGT as the desired SR changes.

Figure 9 BSFC comparison of layouts b (left plot) and d (right plot) (see online version for colours)

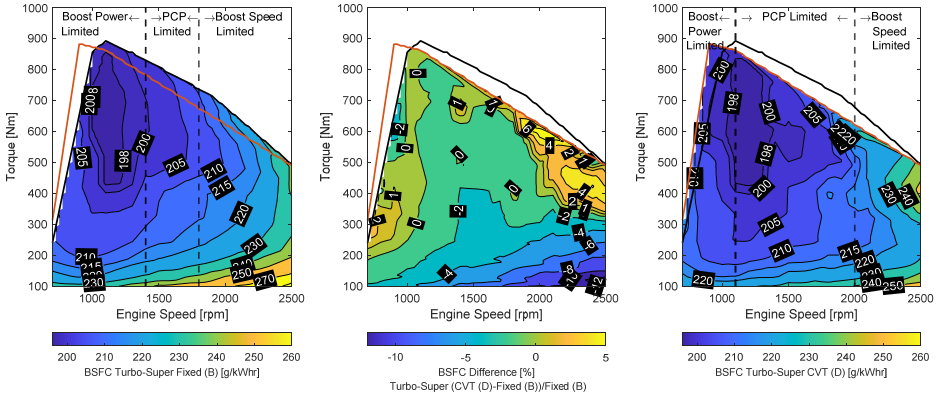

Notes: The middle plot shows the relative percent difference between the layouts, with a negative value corresponding to layout d being more efficient. the fixed drive ratio of layout b requires significant flow recirculation at higher speeds and lower loads, leading to worse efficiency in these regions.

Figure 10 Backpressure valve losses as a fraction of total exhaust energy as calculated by equation (5) (see online version for colours)

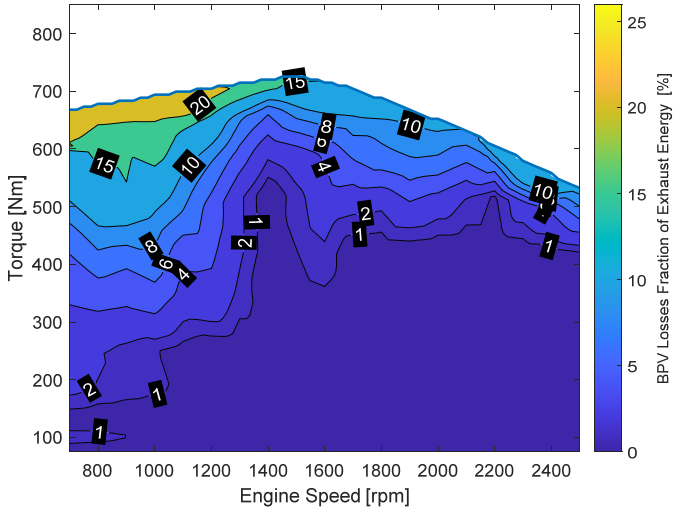

Notes: Higher values mean more energy is lost by the BPV, leading to less energy available for the turbine to recover

Even though they use the same supercharger and turbocharger, the two turbo-super layouts had notably different operating ceilings (Figure 9), with the turbo-super fixed layout generally having a higher peak torque. This higher peak torque was due to the

lower conversion losses of the turbo-super fixed layout compared to the turbo-super CVT layout due to the lack of a variable ratio transmission (Table 3). The variable ratio transmission of the turbo-super CVT layout did, however, improve peak torque at very low engine speeds, where the gearing of the turbo-super fixed layout caused the supercharger to not able to supply sufficient airflow.

While having a fixed drive ratio and the associated lower conversion losses in layout B led to a higher engine efficiency at higher loads and speeds, this speed coupling, and the required recirculation valve, led to efficiency penalties elsewhere for two main reasons. Firstly, recirculating up to two-thirds of the flow through the supercharger means the supercharger was doing excess unnecessary work compressing the intake charge. Secondly, the supercharger was spun faster than necessary in many conditions, causing it to operate at a higher MFR and lower pressure ratio, where it was less efficient. (Figure 11). This second point was the driving factor in the drastically worse efficiency of the turbo-super fixed layout at high speeds and low loads compared to the turbo-super CVT layout. In these conditions, the turbo-super CVT's variable drive ratio allowed for it to operate at more efficient areas of the supercharger map, which, coupled with the lack of a recirculation valve, led to the observed benefits.

Figure 11 Supercharger efficiency map for layouts b and d overlaid with operating points of each layout (see online version for colours)

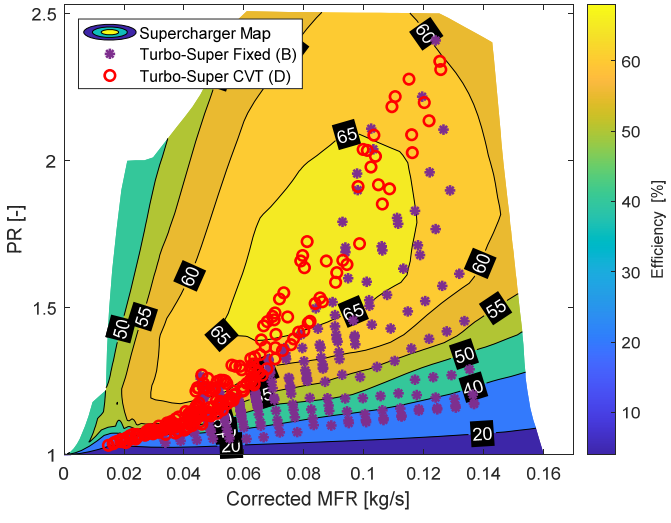

Notes: Layout d generally operates in a more efficient region of the map due to its lack of a recirculation valve.

The conversion losses were the primary drawback of using a variable ratio drive with a supercharger discussed thus far. As discussed previously, it was assumed in this work that the efficiency of the CVT was 88%, an efficiency penalty that was not present in the fixed ratio configuration. This meant that in regions where the fixed supercharger is not bypassing significant flow, its lower conversion losses can lead to higher overall efficiencies, as shown in Figure 9. A more detailed discussion of the influences of airpath losses on engine efficiency is presented in a following section.

7.1 EAT VGT vs. turbo-super CVT

The EAT VGT and turbo-super CVT layouts were the most promising single-stage and dual-stage airpaths investigated, respectively, due to their favourable control characteristics and low overall pumping losses. To better understand the differences between these layouts, the average boost device losses as a function of crank power are compared in Figure 12. This comparison additionally allows for the torque characteristics of each layout to be further investigated. Both layouts made their peak torque below 1300rpm and had similar peak torques. As the engine speed increased, the EAT-VGT layout had a flatter torque curve and ultimately was the more powerful airpath. Since both airpaths were PCP limited for a large portion of their operating range, this increase in brake torque of layout C was directly related to a reduction in airpath losses in these regions.

Across most of the operating range, the EAT VGT had a more efficient boosting system than the turbo-super CVT. Additionally, the EAT VGTs boosting efficiency was primarily load dependent, instead of primarily speed dependent like the turbo-super CVT. To understand why diving deeper into how the various airpath components work together is necessary.

Figure 12 Comparison of losses between layouts c and d (see online version for colours)

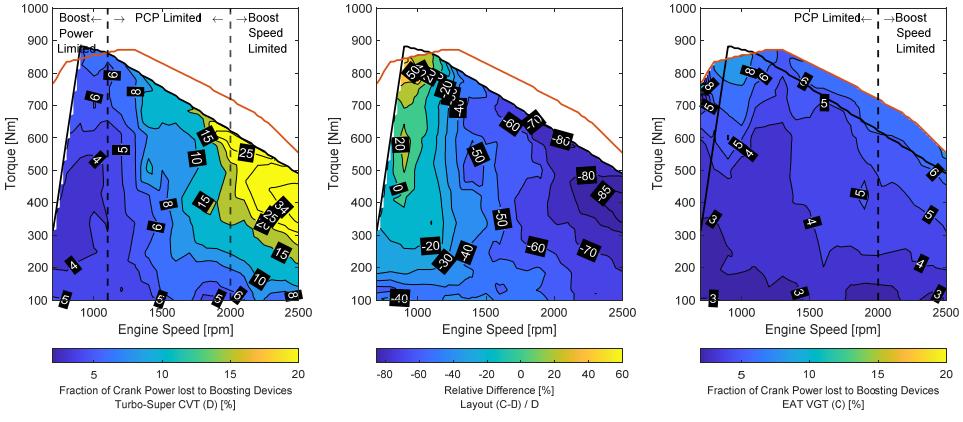

Notes: In these plots, the boosting device losses are calculated as the required crank power to drive all boosting devices, and the crank power is calculated as the power available at the crank neglecting boost device losses. The turbo super CVT layout exhibits a greater speed dependence for losses, while the eat VGT layout exhibits a stronger load dependence on losses. the reduced high load losses of the eat VGT layout compared to the turbo super CVT layout also allow for a higher peak torque without violating the PCP limits of the engine.

In the turbo-super CVT layout, the turbocharger was not coupled to the supercharger by any mechanical or electrical means. This means that any energy recovered by the turbine could only be used to power the compressor. For most of the operating range, there were no significant downsides to this; however, at high speeds and loads, this lack of coupling became problematic. At high speeds and loads, there was a large amount of exhaust energy to recover, and for SR control, the VGT must impose a relatively high restriction on the exhaust. These factors combined to cause the turbine to recover more energy than

the compressor could efficiently use, or use at all, in some cases. This caused the compressor to operate in an inefficient regime of its map or overspeed, leading to a lower peak torque. In the case of the EAT VGT, since the EAT motor must always put energy into the compressor, this high-speed high load case meant that the demands on the EAT motor were lower than they otherwise would be, leading to the higher efficiency compared to the turbo-super CVT layout. The EAT VGT did still overspeed due to the compressor's inability to supply enough air, but this condition occurs at a higher torque.

The turbo-super CVT layout was more efficient at low speeds and high loads. This was due to the differences in the efficient operating regions of a supercharger and turbocharger. In these conditions, the engine operated at a relatively low MFR and a high pressure ratio, a region where turbocharger compressors are prone to surge and have poor efficiency. Additionally, these operating regions had little exhaust energy, meaning the engine had to supply most of the boosting work mechanically or electrically. These factors compounded to make the EAT VGT inefficient in these regions. The supercharger in the turbo-super CVT better adapted to these conditions due to its relatively high efficiency under these operating conditions.

For the rest of the operating range, the EAT VGT had a more efficient airpath than the turbo-super CVT. This is due to a combination of the previously discussed factors and the average efficiency of the various boosting devices (Table 4).

Table 4 Boosting device and conversion efficiencies for layouts C and D, averaged across their operating ranges

	Turbo-super CVT	*EAT VGT*
Turbine [%]	65	64
Compressor [%]	61	67
Supercharger [%]	57	-
Conversion [%]	79	81

Notes: The lower efficiency of the turbo-super CVT devices negates any potential benefits if a two-stage boosting system.

Since both layouts utilised identical turbines, their average turbine efficiencies were similar. However, the other efficiencies of the turbo-super CVT layout were lower than that of the EAT VGT. These differences reduced any potential benefits a two-stage boosting system may have and helped contribute to the discussed results.

7.2 Airpath component efficiency sensitivity study

Given the significant differences in component efficiencies and their influence on overall engine efficiencies that were shown previously, it was desirable to perform a sensitivity study to analyse these relationships further. This study perturbed the efficiencies of the various airpath devices on layouts C and D to determine how these efficiencies influence each other and the engine. Four speed/fuelling conditions (1,100 rpm, 16.2 bar IMEPn, 1,250 rpm 9.2 bar IMEPn, 1,700 rpm 7.3 bar IMEPn, 2,200 rpm 12.2 bar IMEPn) were used to provide a good range of operating conditions. At each speed/load, a 256-point Latin Hypercube was generated and run, which imposed efficiency multipliers of between 0.9 and 1.1 on each factor. All factors in all cases exhibited a linear sensitivity to brake efficiency with an R^2 of > 0.99 and > 0.96 for the EAT VGT and turbo-super CVT

layouts, respectively. EGR component efficiencies were initially included in this study but were omitted from the final results presented in Figure 13 due to their relatively negligible influence on BTE.

Figure 13 Relative influence on brake efficiency of different airpath component efficiencies (see online version for colours)

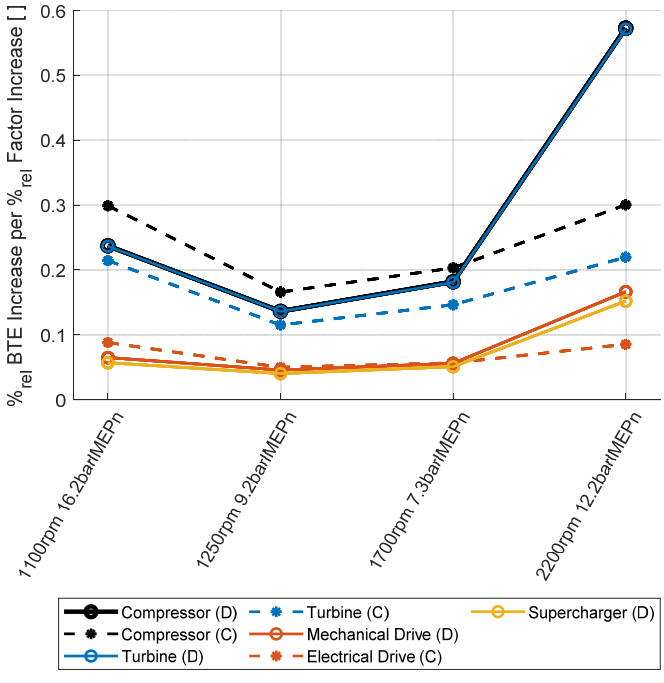

Notes: Each component's efficiency was swept using a multiplier, and the relative change in BTE calculated. This normalises the data and prevents possible skew due to differences in component's baseline efficiency values.

In general, at higher loads, the influence of airpath efficiency on brake efficiency increased due to the increased fraction of indicated power required to drive the airpath. Since the compressor and turbine of the turbo-super CVT (D) were directly coupled with no outside power sources/draws and consumed/recovered the same amount of energy, changing their efficiencies had identical effects on engine efficiency. The same was not valid for the compressor and turbine of the EAT VGT (C) due to the EAT motor. For this airpath, BTE was more sensitive to compressor efficiency than turbine efficiency because the compressor drew more work than the turbine recovered, with the additional energy being supplied by the EAT motor. The influence of the electric drive efficiency of the EAT was also less important than that of the compressor or turbine. This was because the EAT motor always consumed less energy than the compressor or turbine recovered. If the EAT was of a decoupled type with a separate expander/generator and compressor/motor, the importance and influence of conversion efficiencies would be significantly higher. In the case of the mechanical drive of the turbo-super CVT, its efficiency had the same influence on BTE as the supercharger's efficiency. This was because, from the engine's perspective, an increase in efficiency of either item will lead to the same reduction in

parasitic load as the devices were coupled in series. Since the supercharger and mechanical drive had lower energy usage than the turbocharger, they had a lower influence on engine efficiency. The super-turbo CVT layout's turbocharger could influence engine efficiency because a more efficient turbocharger reduced the amount of work required from the supercharger, thereby increasing engine BTE.

These results followed the expected trends for what causes a device's efficiency to have a larger or smaller relative influence on system efficiency. However, this sensitivity study also presents insights into each layout's speed and load dependencies. The two architectures exhibited relatively similar trends for the first three speed/load points. However, at the highest speed/load point, (2,200 rpm 12.2 bar IMEPn), the sensitivity of BTE to compressor and turbine efficiency doubled for the turbo-super CVT layout compared to the other points. This highlights a notable disadvantage of this layout that partially led to the conditions found in Figure 12. Since the supercharger was optimised to maximise efficiency at low-mid speeds, and the turbocharger does not have an electric assist, the supercharger must be operated near its maximum speed and pressure ratio to achieve sufficient boost at this high speed/load point. This is a relatively inefficient area of the map to operate, hurting overall engine performance. In this operating regime, it was better to increase turbine or compressor efficiency than supercharger efficiency, not only due to the higher energy recovered/consumed by the turbocharger but also because an increase in turbine or compressor efficiency moves the operating point of the supercharger to a lower pressure ratio, lower speed, and therefore more efficient region. Overall, even with this high sensitivity, significant efficiency increases would be required for the airpath components of the turbo-super CVT layout to match the efficiency of the EAT VGT layout. Therefore, the EAT VGT layout is proposed as the most promising airpath for this engine architecture.

8 Conclusions

Efficient airpaths with accurate and independent control over intake and exhaust system pressures are needed for OP2S engines. This allows for the engine's scavenging process and internal composition to be controlled and is crucial due to the higher sensitivity to intake and exhaust pressure of an OP2S compared to a conventional four-stroke engine. However, having control over these pressures results in trade-offs between maximising engine efficiency, maintaining airpath simplicity, and maximising the range of scavenging control of the engine.

The two most promising ways identified of allowing for independent pressure control, and therefore scavenging control, are the implementation of either a BPV or a VGT. Using these two scavenging actuators, and a range of compression and expansion devices, four airpaths were further investigated in 1D simulation. Tests were controlled to allow for a direct comparison of pumping losses between layouts and yielded the following conclusions:

- The electric EGR pump has a minor influence on engine efficiency
- Boosting and conversion losses can account for up to a 9% reduction in indicated power
- The single-stage airpaths utilising EATs have the lowest pumping losses

- On the two-stage airpaths, the tested architecture is significantly more sensitive to supercharger sizing when the supercharger is directly driven and does not utilise a CVT
- Airpath selection can have a significant influence on brake torque output

The most promising two-stage turbo-super and single-stage EAT layouts were then further investigated in a comparison of full map pumping work and a sensitivity study of BTE to airpath component efficiencies. It was found that the EAT with VGT had lower overall pumping losses across most of its operating range, with the notable exception of high-load low-speed operation where the turbo-super CVT layout was more favourable. The lower pumping losses across most of the operating range also led to a higher and broader torque ceiling for the EAT with VGT layout. From the sensitivity study, it was found that the trends followed expected results, i.e., the efficiencies of airpath components that required or recovered the greatest amount of power had the largest influence on BTE and that these components should therefore be focused on when investigating how to improve the efficiency of a given airpath. Overall, it is concluded that the EAT with VGT is the most promising airpath of those investigated. It has both lower pumping working and a higher torque ceiling than any other architectures investigated for most of its operating range.

Acknowledgements

This work was supported by the Department of Energy's Vehicle Technologies Office under award number DE-EE0009202.

References

Abani, N., Nagar, N., Zermeno, R., Chiang, M. et al. (2017) 'Developing a 55% BTE commercial heavy-duty opposed-piston engine without a waste heat recovery system', *SAE Technical Paper,* Vol. 2017, No. 1, p.638, DOI:10.4271/2017-01-0638.

Alshammari, F., Karvountzis-Kontakiotis, A., Pesyridis, A. and Usman, M. (2018) 'Expander technologies for automotive engine organic rankine cycle applications', *Energies*, Vol. 11, No. 7, p.1905, DOI:10.3390/en11071905.

Amann, C. (1987) *Selecting Components for a Compound Low-Heat-Rejection Diesel for Light-Duty Use*, SAE Technical Paper 870025, DOI: 10.4271/870025.

Andruskiewicz, P., Durrett, R. and Najt, P. (2021a) 'Low-load expander deactivation studies for a light-duty single-shaft piston-compounded engine', *International Journal of Engine Research*, Vol. 22, No. 3, pp.699–710, DOI:10.1177/1468087419886501.

Andruskiewicz, P., Durrett, R., Gopalakrishnan, V. and Najt, P. (2021b) 'Dual-compression, dual-expansion piston engine assessment and optimization', *International Journal of Engine Research*, Vol. 22, No. 3, pp.791–804, DOI:10.1177/1468087419879609.

Andruskiewicz, P., Durrett, R., Gopalakrishnan, V., Narayanaswamy, K. and Najt, P. (2021c) 'Exploring light-duty internal combustion engine boosting and exhaust compounding strategies', *International Journal of Engine Research,* Vol. 22, No. 3, pp.711–730, DOI:10. 1177/1468087419882141.

Bassett, M., Hall, J., Hibberd, B., Borman, S. et al. (2016) 'Heavily downsized gasoline demonstrator', *SAE Int. J. Engines*, Vol. 9, No. 2, pp.729–738, DOI:10.4271/2016-01-0663.

Blair, G.P. (1996) *Design and Simulation of Two-Stroke Engines*, Society of Automotive Engineers, Inc., Warrendale, PA.

Boretti, A. (2019) 'Half/full toroidal, single/double roller, CVT based transmission for a super-turbo-charger', *Proceedings of Engineering and Technology Innovation*, Vol. 11, pp.1–11.

Chen, S. and Flynn, P. (1965) *Development of a Single Cylinder Compression Ignition Research Engine*, SAE Technical Paper, p.650733, DOI:10.4271/650733.

Gainey, B., Bhatt, A., O'Donnell, P., Prucka, R., Filipi, Z., Redon, F. and Lawler, B. (2022) 'Experimental study of the impact of scavenging efficiency on diesel combustion in an opposed-piston two-stroke engine', *International Journal of Engine Research*, DOI:10.1177/14680874221135007.

Galindo, J., Serrano, J.R., Climent, H. and Varnier, O. (2010) 'Impact of two-stage turbocharging architectures on pumping losses of automotive engines based on an analytical model', *Energy Conversion and Management*, Vol. 51, No. 10, pp.1958–1969, https://doi.org/10.1016/j.enconman.2010.02.028.

Herold, R.E., Wahl, M.H., Regner, G., Lemke, J.U. and Foster, D.E. (2011) *Thermodynamic Benefits of Opposed-Piston Two-Stroke Engines,* No. 2011-01-2216. SAE Technical Paper, DOI: 10.4271/2011-01-2216.

Heywood, J.B. and Sher, E. (1999) *The Two-Stroke Cycle Engine: Its Development, Operation, and Design*, Taylor & Francis Group, New York, NY.

Indig, H. and Haman, A. (1985) *Experimental Analysis of an Inwardly-Opposed Piston Engine*, SAE Technical Paper 850362, DOI:10.4271/850362.

Kalke, J., Opaliński, M. and Szczeciński, M. (2014) 'Opposed-Piston engines: the future of internal combustion engines?', *PhD Interdisciplinary Journal*, Vol. 1, No. 1, pp.175–184.

Lee, W., Schubert, E., Li, Y., Li, S., Bobba, D. and Sarlioglu, B. (2017) 'Overview of electric turbocharger and supercharger for downsized internal combustion engines', in *IEEE Transactions on Transportation Electrification*, Vol. 3, No. 1, pp.36–47, March 2017, DOI: 10.1109/TTE.2016.2620172.

Lion, S., Michos, C.N., Vlaskos, I., Rouaud, C. and Taccani, R. (2017) 'A review of waste heat recovery and organic rankine cycles (ORC) in on-off highway vehicle heavy duty diesel engine applications', *Renewable and Sustainable Energy Reviews*, Vol. 79, No. 1, pp.691–708, DOI:10.1016/j.rser.2017.05.082.

Liu, Y., Zhang, F., Zhao, Z., Cui, T., Zuo, Z. and Zhang, S. (2017) 'The effects of pressure difference on opposed piston two stroke diesel engine scavenging process', *Energy Procedia*, pp.1172–1178, DOI: 10.1016/j.egypro.2017.12.374.

Ma, F., Zhang, L. and Su, T. (2018) 'simulation modeling and optimization of uniflow scavenging system parameters on opposed-piston two-stroke engines', *Energies*, Vol. 11, p.940, DOI:10.3390/en11040940.

Ma, F., Zhao, C., Zhang, S. and Wang, H. (2015) *Scheme Design and Performance Simulation of Opposed-Piston Two-Stroke Gasoline Direct Injection Engine*, SAE Technical Paper, DOI:10.4271/2015-01-1276.

Mattarelli, E., Cantore, G., Rinaldini, C.A. and Sacioli, T. (2018) 'Combustion system development of an opposed piston 2-stroke diesel engine', *Energy Procedia*, Vol. 126, pp.1003–1010, DOI: 10.1016/j.egypro.2017.08.268.

Mattarelli, E., Rinaldini, C., Savioli, T., Cantore, G. et al. (2017) *Scavenge Ports Optimization of a 2-Stroke Opposed Piston Diesel Engine*, SAE Technical Paper, DOI:10.4271/2017-24-0167.

Mazuro, P. and Kozak, D. (2022) 'Experimental investigation on the performance of the prototype of aircraft opposed-piston engine with various values of intake pressure', *Energy Conversion and Management*, Vol. 269, DOI: 10.1016/j.enconman.2022.116075.

McBroom, S., Smithson, R., Urista, R. and Chadwell, C. (2012) 'Effects of variable speed supercharging using a continuously variable planetary on fuel economy and low speed torque', *SAE Int. J. Engines*, Vol. 5, No. 4, pp.1717–1728, DOI: 10.4271/2012-01-1737.

Naik, S., Redon, F., Regner, G. and Koszewnik, J. (2015) *Opposed-Piston 2-Stroke Multi-Cylinder Engine Dynamometer Demonstration*, SAE Technical Paper, DOI:10.4271/2015-26-0038.

O'Donnell, P., Gandolfo, J., Gainey, B., Vorwerk, E. et al. (2022) *Effects of Port Angle on Scavenging of an Opposed Piston Two-Stroke Engine* SAE Technical Paper 2022-01-0590.

Orr, B., Akbarzadeh, A., Mochizuki, M. and Singh, R. (2016) 'A review of car waste heat recovery systems utilising thermoelectric generators and heat pipes', *Applied Thermal Engineering*, Vol. 101, No. 1, pp.490–495, DOI:10.1016/j.applthermaleng.2015.10.081.

Patil, S., Ghazi, A., Redon, F., Sharp, C., Schum, D. and Headley, J. (2018) *Cold start HD FTP Test Results on Multi-Cylinder Opposed-Piston Engine Demonstrating Rapid Exhaust Enthalpy Rise to Achieve Ultra Low NOx*, No. 2018-01-1378. SAE Technical Paper, DOI:10.4271/2018-01-1378.

Pirault, J-P. and Flint, M.L.S. (2010) *Opposed Piston Engines: Evolution, Use, and Future Applications*, SAE International, Warrendal, PA.

Redon, F., Sharma, A. and Headley, J. (2015) *Multi-Cylinder Opposed Piston Transient and Exhaust Temperature Management Test Results*, SAE Technical Paper 2015-01-1251, DOI:10.4271/2015-01-1251.

Regner, G., Herold, R.E., Wahl, M.H., Dion, E., Redon, F., Johnson, D., Callahan, B.J. and McIntyre, S. (2011) 'The achates power opposed-piston two-stroke engine: performance and emissions results in a medium-duty application', *SAE International Journal of Engines*, Vol. 4, No. 3, pp.2726–2735, DOI: 10.4271/2011-01-2221.

Ricardo, M.B., Apostolos, P. and Yang, M.Y. (2011) 'Overview of boosting options for future downsized engines', *Sci. China Tech. Sci.*, Vol. 54, pp.318–331, DOI: 10.1007/s11431-010-4272-1.

Rizk, W. (1958) 'Experimental studies of the mixing processes and flow configurations in two-cycle engine scavenging', *Proceedings of the Institution of Mechanical Engineers*, Vol. 172, No. 1, pp.417–437, DOI:10.1243/PIME_PROC_1958_172_037_02.

Salvi, A., Hanson, R., Zermeno, R., Regner, G., Sellnau, M. and Redon, F. (2022) 'Initial results on a new light-duty 2.7L opposed-piston gasoline compression ignition multi-cylinder engine', *ASME. J. Energy Resour. Technol.*, Vol. 144, No. 9, p.92302, DOI: 10.1115/1.4053518.

Sekar, R. and Kamo, R. (1983) *Positive Displacement Compounding of A Heavy Duty Diesel Engine*, Nasa Report NAS, Vol. 1, No. 26, p.168286.

Sekar, R., Kamo, R. and Wood, J. (1984) *Advanced Adiabatic Diesel Engine for Passenger Cars*, SAE Technical Paper 840434, DOI:10.4271/840434.

Serrano, J.R., Arnau, F.J., Dolz, V. et al. (2008) 'Analysis of the capabilities of a two-stage turbocharging system to fulfil the US2007 anti-pollution directive for heavy duty diesel engines', *Int. J. Automot. Technol.*, Vol. 9, pp.277–288, DOI:10.1007/s12239-008-0034-5.

Sokolsky, S. and Major, J. (2019) 'Advanced combat engine militarization and commercialization study', *Proceedings of the Ground Vehicle Systems Engnineering and Technologoy Symposium (GVSETS)*, NDIA, Novi, MI.

Sturm, S., Schmidt, S. and Kirchberger, R. (2018) *Overview of Different Gas Exchange Concepts for Two-Stroke Engines*, SAE Technical Paper, DOI:10.4271/2018-32-0041.

Timoney, S. (1969) *High Pressure Turbocharging of Two-Stroke Engines*, SAE Technical Paper 690747, DOI:10.4271/690747.

Turner, J., Popplewell, A., Marshall, D., Johnson, T. et al. (2015) 'Super gen on ultraboost: variable-speed centrifugal supercharging as an enabling technology for extreme engine downsizing', *SAE Int. J. Engines*, Vol. 8, No. 4, pp.1602–1615, DOI:10.4271/2015-01-1282.

Verbelen, F., Derammelaere, S., Sergeant, P. and Stockman, K. (2017) 'Visualizing the efficiency of a continuously variable transmission', in *Energy Efficiency in Motor Driven Systems EEMODS 2017.*

Witzky, J., Meriwether, R. and Lux, F. (1965) *Piston-Turbine-Compound Engine — A Design and Performance Analysis*, SAE Technical Paper 650632, DOI:10.4271/650632.

Woschni, G. (1967) *A Universally Applicable Equation for the Instantaneous Heat Transfer Coefficient in the Internal Combustion Engine*, SAE Technical Paper, Vol. 670931, DOI:10.4271/670931.

Young, A., Turner, J. and Head, R. (2021) *Turbocompounding the Opposed-Piston 2-Stroke Engine*, SAE Technical Paper 2021-01-0636, DOI:10.4271/2021-01-0636.

Zhang, Q., Pennycott, A. and Brace, CJ. (2013) 'A review of parallel and series turbocharging for the diesel engine', in *Proceedings of the Institution of Mechanical Engineers, Part D: Journal of Automobile Engineering*, Vol. 227, No. 12, pp.1723–1733, DOI:10.1177/09544070 13492108.

Zheng, M., Reader, G.T. and Hawley, J.G. (2004) 'Diesel engine exhaust gas recirculation–a review on advanced and novel concepts', *Energy Conversion and Management*, Vol. 45, No. 6, pp.883–900, https://doi.org/10.1016/S0196-8904(03)00194-8.

Definitions/abbreviations

AFR	Air to fuel ratio
BMEP	Brake mean effective pressure
BPV	Backpressure valve
BSFC	Brake specific fuel consumption
BTE	Brake thermal efficiency
CFD	Computational fluid dynamics
CVT	Continuously variable transmission
dP	Cycle-averaged difference between the intake manifold or chest pressure, and the exhaust manifold or chest pressure
EGR	exhaust gas recirculation
ERR	Exhaust residual ratio
EAT	Electrically-assisted turbocharger
ITE	Indicated thermal efficiency
OP2S	Opposed piston two stroke
PCP	Peak cylinder pressure
SC	Supercharger
SE	Scavenging efficiency
SR	Scavenging ratio
TDCf	Top dead centre firing
TE	Trapping efficiency
VGT	Variable geometry turbine

Appendix A

Scavenging definitions

Scavenging efficiency (SE)

SE is the mass fraction of delivered mixture retained compared to total trapped mass in cylinder at port/valve closure and will always be less than or equal to 1. This is a critical metric for the comparison of scavenging strategies as it describes how much fresh charge displaces residual, as shown in (1). (Blair, 1996) This additionally means that the inverse of this metric is equivalent to the amount of internal residual in the cylinder.

Scavenging ratio (SR)

SR compares the mass of the delivered mixture to the total trapped mass at port/valve closure as shown in (2). A SR > 1 implies that the engine is ingesting more mixture than can be trapped in its cylinder and that short-circuiting occurred. Ideally, SR will be equal to SE, as this implies that the engine is not short-circuiting. (Blair, 1996)

Trapping efficiency (TE)

Trapping efficiency is used to define the portion of delivered mixture that is trapped in the cylinder at port/valve closure and will always be less than or equal to 1. This metric is important because it describes the relationship between SE and SR as shown in (A1), additionally its inverse is the fraction of charge that is short-circuited (Blair, 1996). Generally, a higher TE implies lower pumping losses due to less short-circuiting.

$$\mathrm{TE} = \frac{\text{Mass of deliveredmixture retained}}{\text{Mass of delivered mixture}} = \frac{\mathrm{SE}}{\mathrm{SR}} \tag{A1}$$

Perfect displacement scavenging

In perfect displacement scavenging, all of the delivered mixture is trapped, i.e., there is no short-circuiting. Additionally, all of the delivered mixture perfectly displaces the same mass of residual in-cylinder mixture from the previous scavenging event. (Pirault and Flint, 2010). More rigorously this means that the mass of delivered mixture retained is equal to the mass of delivered mixture and therefore TE = 1 = SE/SR. This relationship leads to the linear relationship with a slope of 1 on the graph in Figure B1. This curve saturates at a SE of 1, because at that point all trapped mass at IPC from the delivered mixture, and there is no residual in-cylinder mixture remaining, so it is impossible to further reduce the amount of residual in-cylinder mixture retained. The closer the SE-SR relationship of an engine approaches this curve, the less short-circuiting is present, and theoretically the lower the pumping work will be. (Heywood and Sher, 1999). From (B1) and Figure B1 it is also shown that for a given architecture there will be a SR below which the engine's SE = SR, i.e., its scavenging is perfect displacement. This is due to the finite time it takes for the delivered mixture to reach the exhaust port during the scavenging process. Architectures that employ uniflow scavenging, such as OP2Ss, generally are perfect displacement to a higher SR, leading to a more efficient scavenging process compared to loop flow or cross flow processes (Rizk, 1958).

Perfect mixing scavenging

In perfect mixing scavenging, the delivered mixture perfectly mixes instantaneously with the in-cylinder mixture. The charge being exhausted is therefore a homogenous mixture of the delivered mixture and in-cylinder residuals, with a ratio equal to that of the in-cylinder mixture at that point in time. Numerically this means that the TE can be described as in (A2) (Blair, 1996).

$$TE = \frac{1 - e^{-SR}}{SR} \tag{A2}$$

The closer the SE-SR relationship of an engine approaches this curve, the more short-circuiting will be present, and theoretically the higher the pumping work will be.

Appendix B

SE-SR correlations

To generate a SE-SR correlation, experimental or 3D CFD data on engine scavenging at a range of operating conditions is collected. This data is then fit to an equation such (B1), which is used for this work.

$$SE = \begin{cases} y_0 + A_1 e^{-\tau_1 SR} + A_2 e^{-\tau_2 SR}, & SR > \beta_1 \\ SR, & SR \leq \beta_1 \end{cases} \tag{B1}$$

where y_0, A_1, A_2, β_1, β_2, τ_1, and τ_2 are fit coefficients

Figure B1 3D CFD derived SE-SR correlation for an OP2S shown in relation to the perfect displacement and perfect mixing curves, as well as fired and motored experimental data covering a range of 700–2,200 rpm and 0.25–13.25 bar brake mean effective pressure (BMEP) (see online version for colours)

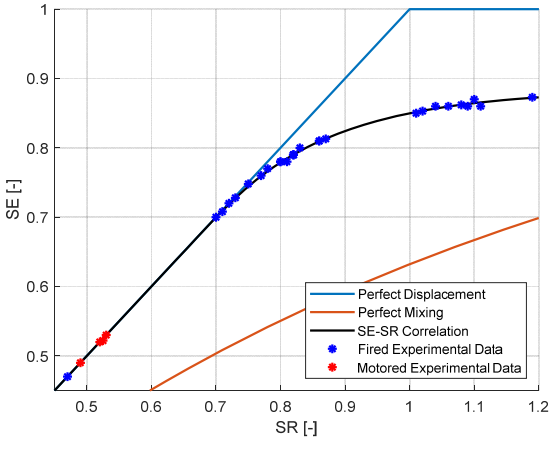

Notes: An SE-SR correlation that is closer to the perfect displacement line is generally better.

The SE-SR correlation for an engine is generally shown in conjunction with perfect displacement and perfect mixing curves. These curves are derived from theoretical scavenging models and roughly bound the scavenging performance of a two-stroke engine. Where an engine falls between these two curves can provide insight on its scavenging process (Blair, 1996). An example SE-SR correlation for an OP2S is shown in Figure B1, along with perfect displacement and perfect mixing lines. Fired and motoring data of an experimental OP2S is also included for a range of operating conditions, displaying the validity of using an SE-SR correlation to represent scavenging performance.

While SE-SR correlations are useful tools for modelling engine scavenging performance, they do have some notable limitations: Since the parameters used to generate this correlation are spatially and temporally averaged, an SE-SR correlation can't provide detailed information into what is causing the engine to scavenge a particular way. Generating this detail requires higher fidelity modelling such as 3D CFD. Additionally, a SE-SR correlation is only valid for a particular engine geometry. Parameters such as crank lead, piston shape, port shape, and some manifold or chest parameters can have large influences on the shape of an SE-SR correlation, necessitating the correlation to be remade (Ma et al., 2018, 2015, Sturm et al., 2018).

Remaking this correlation generally requires coupling 3D CFD and 1D simulation (O'Donnell et al., 2022). In this coupling 1D simulation provides boundary conditions, such as temperature and pressure, to 3D open cycle CFD. The open cycle simulation is then run and used to generate a new SE-SR correlation for use in the 1D simulation. Generally, 3–5 operating conditions are simulated to generate sufficient data to fit a SE-SR correlation. This process is repeated until convergence is met between models, i.e., the new boundary conditions from 1D simulation do not significantly change the predicted scavenging in 3D simulation. While this is a time-intensive process, once complete the 1D simulation can be accurately run across its speed load range, and modifications can be made to things such as boost device sizing without further use of open cycle simulation. That being said, there are limitations to what can be changed architecturally on the model before it is necessary to repeat the process of generating a new SE-SR correlation as described previously.